Journal of ELECTRONIC MATERIALS, Vol. 42, No. 6, 2013
DOI: 10.1007/s11664-013-2475-5

Thermal Cycling Reliability of Sn-Ag-Cu Solder Interconnections—Part 2: Failure Mechanisms

JUSSI HOKKA,[1,2] TONI T. MATTILA,[1] HONGBO XU,[1] and MERVI PAULASTO-KRÖCKEL[1]

1.—Department of Electronics, Aalto University, 00076 Aalto, Finland. 2.—e-mail: jussi.hokka@aalto.fi

Part 1 of this study focused on identifying the effects of (i) temperature difference (ΔT), (ii) lower dwell temperature and shorter dwell time, (iii) mean temperature, (iv) dwell time, and (v) ramp rate on the lifetime of ball grid array (with 144 solder balls) component boards. Based on the characteristic lifetime, the studied thermal cycling profiles were categorized into three groups: (i) highly accelerated conditions, (ii) moderately accelerated conditions, and (iii) mildly/nonaccelerated conditions. In this work, the observed differences in component board lifetime are explained by studying the failure mechanisms and microstructural changes that take place in the three groups of loading conditions. It was observed that, under the standardized thermal cycling conditions (highly accelerated conditions), the networks of grain boundaries formed by recrystallization provided favorable paths for cracks to propagate intergranularly. It is noteworthy that the coarsening of intermetallic particles was strong in the recrystallized regions (the cellular structure had disappeared completely in the crack region). However, under real-use conditions (mildly/nonaccelerated conditions), recrystallization was not observed in the solder interconnections and cracks had propagated transgranularly in the bulk solder or between the intermetallic compound (IMC) layer and the bulk solder. The real-use conditions showed slight coarsening of the microstructure close to the crack region, but the solder bulk still included finer IMC particles and β-Sn cells characteristic of the as-solidified microstructures. These findings suggest that standardized thermal cycling tests used to assess the solder interconnection reliability of BGA144 component boards create failure mechanisms that differ from those seen in conditions representing real-use operation.

Key words: Reliability, thermal cycling, thermal shock, microstructure, recrystallization, accelerated lifetime test

INTRODUCTION

Electronic devices experience significant changes in temperature during normal operation due to internal heat dissipation and variation of the ambient temperature. As component boards inside are exposed to temperature changes, strains and stresses concentrate in the solder interconnections as the natural expansion/contraction of the printed wiring board (PWB) is restricted by the packages. Thermomechanical reliability is typically characterized by performing thermal cycling tests in which various parameters such as dwell time, ramp rate, and temperature extremes are used to accelerate real operation conditions. There are, however, risks involved with all accelerated tests: Do the failure modes and mechanisms remain the same when the loading conditions are harshened to produce higher acceleration? The purpose of this paper is to answer this question.

(Received July 12, 2012; accepted January 7, 2013; published online February 23, 2013)

The reliability of solder interconnections has been studied for several decades, but the shift from Sn-Pb solders to lead-free solders has made comprehensive reliability reassessments necessary. It is well known that, under thermomechanical loading, cracking of solder interconnections is strongly influenced by the microstructures formed during soldering and their evolution during operation. However, it has been observed that the microstructural changes in Sn-rich lead-free solders are markedly different from those observed in Sn-Pb solders.[1] Nevertheless, the same thermomechanical test parameters that have been determined and designed for eutectic Sn-Pb solders are still used even though the solder has been changed to Sn-rich lead-free solder.

It is well known that, in eutectic Sn-Pb solder, the as-solidified microstructure is divided into solidification colonies in which the Pb-rich and the Sn-rich phase are clearly distinguishable. Shear loading of ball grid array (BGA) solder interconnections, for example, produces shear strain that is localized in bands of maximum shear parallel to the solder–pad interface. This inhomogeneous deformation induces localized coarsening of the eutectic structure, and eventually fatigue cracks propagate through the coarsened bands along boundaries between the as-solidified and coarsened microstructure (see, e.g., Refs. 2,3 for more detail). However, microstructural observations of failed Sn-Ag-Cu solder interconnections exposed to accelerated thermal cycling tests have indicated that the microstructures of solder interconnections change distinctly before cracking (see, e.g., Refs. 4–6). The as-solidified microstructures of Sn-rich solder interconnections are usually composed of few, large Sn colonies distinguished by high-angle boundaries.[7,8] Under dynamic loading conditions, such as thermal cycling tests (between –40°C and +125°C), the solidification colonies transform locally into more or less equiaxed grain structures by recrystallization, which forms a continuous network of grain boundaries that provide favorable sites for cracks to nucleate and propagate, with less energy consumption than in the as-solidified microstructures.[8–10] Similar observations were later made by other authors.[11–14]

The purpose of this study is to perform a critical reevaluation of the thermal cycling parameters that are currently employed in standardized thermal cycling tests by comparing the failure modes/mechanisms observed in various accelerated test conditions and in conditions simulating real-use operation. The study has been divided into two parts. In part 1, the effects of (i) temperature difference (ΔT), (ii) lower extreme temperature, (iii) mean temperature, (iv) dwell time, and (v) ramp rate on BGA144 component boards were studied from the perspective of lifetime statistics and acceleration of test conditions. Here, in part 2, the objective is to provide further insight into the observed differences in component board lifetime based on thorough examination of the physical failure mechanisms. In particular, the mechanisms by which failure of Sn-rich lead-free solder interconnections takes place under different test conditions and their correlation with real-use failures are not yet fully understood. Therefore, in the following, we place emphasis on the microstructural differences observed in the course of the thermal cycling test profiles (producing different rates of acceleration) and pay attention to nucleation and propagation of cracks under each condition. The ultimate objective is to provide means to develop more meaningful methods of reliability assessment for electronic products.

EXPERIMENTAL PROCEDURES

The package used in the study was a 12 mm × 12 mm chip-scale packaged ball grid array (BGA) with 144 Sn-3.0Ag-0.5Cu solder balls with 800 μm pitch and 500 μm ball diameter (Fig. 1). There was no under bump metallization between the solder balls and the copper pads. The Cu soldering pads of the printed wiring boards (eight-layer build-up FR4 structure) were coated with organic solderability preservative (Cu | OSP). More details about the board assemblies can be found in part 1 of this study.

The component boards were thermally cycled using different test parameters (Table I). The different profiles are denoted as follows to indicate the test condition applied: (1) the ramp rate [TC for temperature cycling (<20°C/min), TS for thermal shock (>20°C/min)], (2) the temperature difference between the two temperature extremes (ΔT), (3) the mean temperature, and (4) the dwell time; for

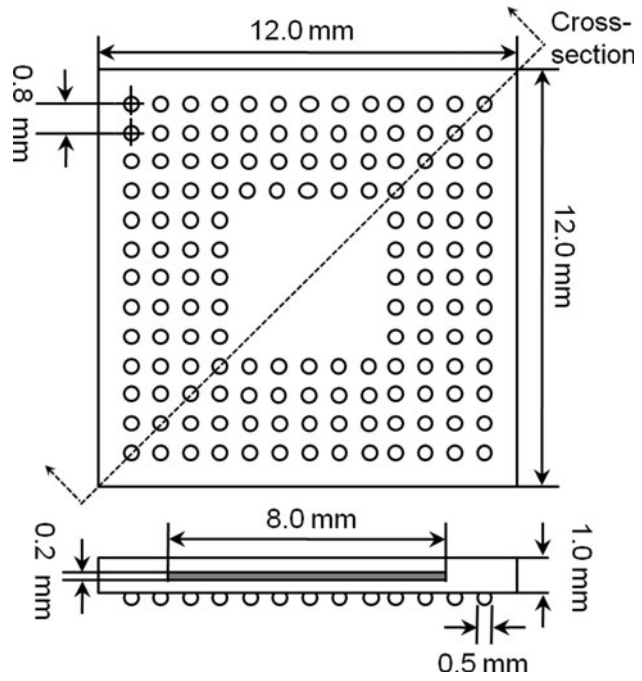

Fig. 1. Layout and dimensions of the component package. Dashed line indicates the direction of the prepared cross-sections.

Table I. Test parameters of the conducted thermal cycling tests and estimates of the Weibull parameters

Thermal profile	Lower dwell [°C]	Upper dwell [°C]	Dwell-time upper / lower [min]	Ramp-rate up / down [°C/min]	Total cycle time [min]	Weibull η (cycles)	Weibull η (hours)	Weibull β	Acceleration class
TC165-42.5C-D0	-40	125	0 / 0	8 / -8	42	7 388	5 172	4.1	High
TC165-42.5C-D30	-40	125	30 / 30	8 / -8	102	8 797	14 956	3.3	High
TS165-42.5C-D0	-40	125	0 / 0	24 / -24	14	5 117	1 194	9.6	High
TS165-42.5C-D5	-40	125	5 / 5	24 / -24	24	8 498	3 399	7.1	High
TS165-42.5C-D10	-40	125	10 / 10	24 / -24	34	4 436	2 514	6.3	High
TS165-42.5C-D15	-40	125	15 / 15	24 / -24	44	3 617	2 652	3.1	High
TS165-42.5C-D30	-40	125	30 / 30	24 / -24	74	6 970	8 596	5.7	High
TS165-76C-D10/0	-40	125	10 / 0	24 / -24	24	8 673	3 469	6.9	High
TS130-60C-D10	-5	125	10 / 10	26 / -26	30	8 312	4 156	2.4	High
TC100-75C-D15	25	125	15 / 15	2 / -2	130	13 626	29 523	4.9	Moderate
TS130-0C-D10	-65	65	10 / 10	26 / -26	30	~ 35 000	~ 17 500	-	Mild
TC50-54C-D24/14	25	75	24 / 14	4 / -2	75	>> 21 000	>> 26 250	-	Mild

Red color (first nine profiles) indicates characteristic lifetime of less than 10,000 cycles, yellow (10th profile) of less than 20,000 cycles, and green (profiles 11 and 12) of over 20,000 cycles. The different profiles are identified by codes that indicate the test condition as follows: (1) the ramp rate [TC for temperature cycling (<20°C/min), TS for thermal shock (>20°C/min)], (2) the temperature difference between the two temperature extremes (ΔT), (3) the time-weighed temperature of the cycle, and (4) the dwell time.

example, "TS165-42.5C-D10" means that the test condition was thermal shock with a temperature difference of 165°C between the temperature extremes, mean temperature of 42.5°C, and dwell time at the temperature extremes of 10 min.

To inspect the microstructural evolution and to study the development of cracks, nonmonitored component boards were placed in the test chambers. Four components were removed from the test chamber every 100 cycles until 1000 cycles, and every 250 or 500 cycles thereafter until all electrically monitored components showed failure (20% increase from the initial resistance of the daisy-chain network was used as the criterion for failure). The thermally cycled samples were cut with a low-speed diamond saw along the diagonal axis of the package so that the cross-section contained two groups of four symmetrically located interconnections (Fig. 1). To reveal the microstructure and to study the failure modes, the cross-sections were prepared by standard metallographic techniques. The cross-sections were polished carefully to remove artifacts introduced by grinding. The cross-sections were analyzed by optical microscopy (BX60; Olympus) and scanning electron microscopy (6335F; JEOL). Cross-polarized light was used in the optical microscopy to inspect interconnection microstructural changes such as recrystallization. Crystal orientations and relative misorientations were quantified with the help of orientation imaging microscopy (OIM) by employing electron backscatter diffraction (EBSD).

Samples for fractographic inspection were prepared by peeling off the packages from the printed wiring boards of the cross-sectioned specimens that were first used for inspections of crack propagation and microstructural changes. The fracture surfaces were inspected by employing scanning electron microscopy. The fracture surfaces produced during thermal cycling were distinguished by comparing the crack length of the interconnections measured during the inspections of the cross-sections with the features of fractured surfaces produced during peeling.

RESULTS

The lifetimes of the component boards under the different test parameters are presented in Table I with the help of the estimated Weibull parameters η (characteristic lifetime in cycles and hours) and β (shape parameter). It can be seen that the component board lifetimes differ significantly with the change of the parameters (from 3617 cycles to ~35,000 cycles). Based on the characteristic lifetime, the profiles were categorized into three groups: (i) highly accelerated conditions (red), (ii) moderately accelerated conditions (yellow), and (iii) mildly/nonaccelerated conditions (green). Here the focus is placed on (i) explaining the observed differences in characteristic lifetime by studying the failure mechanisms, and (ii) studying the differences in the failure mechanisms, especially between the highly accelerated and mildly/nonaccelerated conditions. In the following, the failure mechanisms are discussed from the point of view of microstructural evolution and crack propagation.

Inspections of the failed component boards showed that, under all thermal cycling conditions, the primary failure site, i.e., the location of a failure that caused electrical failure of the daisy-chain network, was cracking of the solder near the package-side

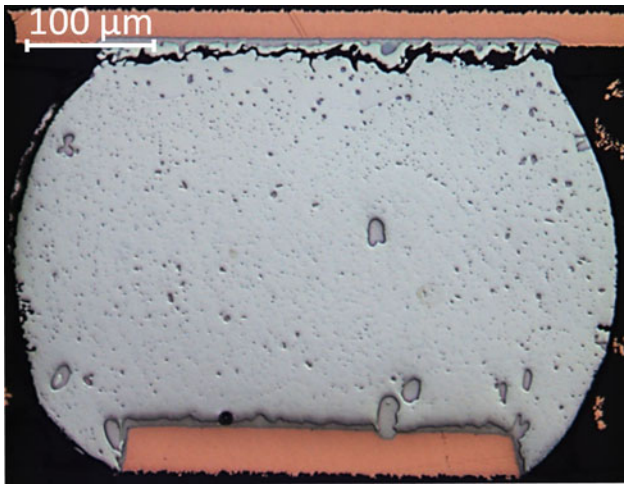

Fig. 2. The primary failure site observed in a solder interconnection after exposure to thermal cycling.

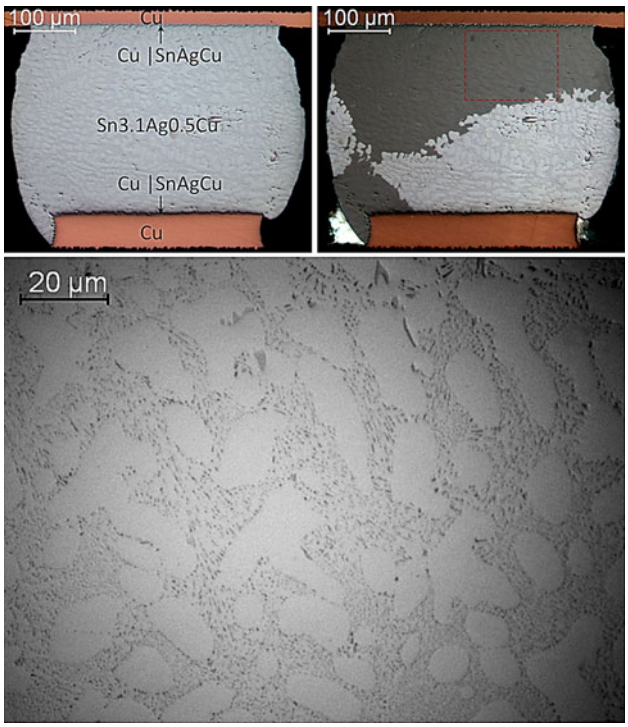

Fig. 3. A bright light image and a polarized light image showing the as-solidified microstructure of an as-soldered interconnection. Dashed box indicates the location of the magnification. The after-reflow composition of the interconnections was calculated as Sn-3.1Ag-0.5Cu.

interfacial regions of the interconnections. Occasionally, a small portion of the entire length of the crack path was located at the interface between the intermetallic layers and the bulk solder on the package side, but such observations were very rare. Cracks on the PWB side of the interconnections were also observed occasionally, but they were not observed to have propagated entirely through the interconnections. Figure 2 shows a micrograph that illustrates the primary failure site under the different thermal cycling conditions.

Evolution of Microstructures

The as-solidified microstructures of the tin-rich solder interconnections were composed of few large solidification colonies of relatively uniformly oriented β-Sn cells, as shown in Fig. 3. The cellular structure is clearly distinguishable as the cells are surrounded by secondary eutectic regions composed of uniformly distributed fine Cu_6Sn_5 and Ag_3Sn particles in the β-Sn matrix. However, in the course of thermal cycling the microstructures started to evolve. It was observed that there is a clear difference in the microstructural evolution between the highly accelerated (red lifetime group) and the mildly/nonaccelerated conditions (green lifetime group; Table I). Therefore, in the following, the observations are discussed separately, starting with the red lifetime group.

It has been observed earlier that, under standard accelerated test conditions, there are two different stages of evolution that cause the observed changes of microstructures in the stress concentration regions: first, coarsening of the intermetallic compound (IMC) particles and tin cells is accompanied by gradual rotation of small volumes by recovery and, later on, the discontinuous change of microstructures by recrystallization.[6] In the failure analysis of the component boards that were exposed to the highly accelerated test conditions (red lifetime group), the change in the microstructure was first observed in the strain concentration regions in the edges of the solder interconnections (i.e., corner regions of a cross-section). Such changes can be observed already after a few hundred load cycles. In the strain concentration regions, the tin cells begin to rearrange by gradual coalescence of tin cells and coarsening of intermetallic particles. The eutectic regions around the tin cells disappear gradually (Fig. 4a, b), and in the course of thermal cycling a network of low-angle boundaries emerges, being produced by recovery (see Refs. 6,13,15 for more details). It is not clear, however, how soon after the start of the test the low-angle boundaries were formed, since not all of the removed samples were analyzed by orientation imaging microscopy, but in our study they were clearly identified in the samples that were removed after 1000 cycles.

The aforementioned microstructural evolution proceeds until the microstructures are transformed discontinuously by recrystallization. The solidification colonies are transformed into an equiaxed grain structure with a network of high-angle grain boundaries surrounding the recrystallized grains. Figure 5 illustrates the formation of low-angle grain boundaries, which can be seen at the PWB-side interface of the solder interconnection. On the other hand, the component-side interface and the crack region are

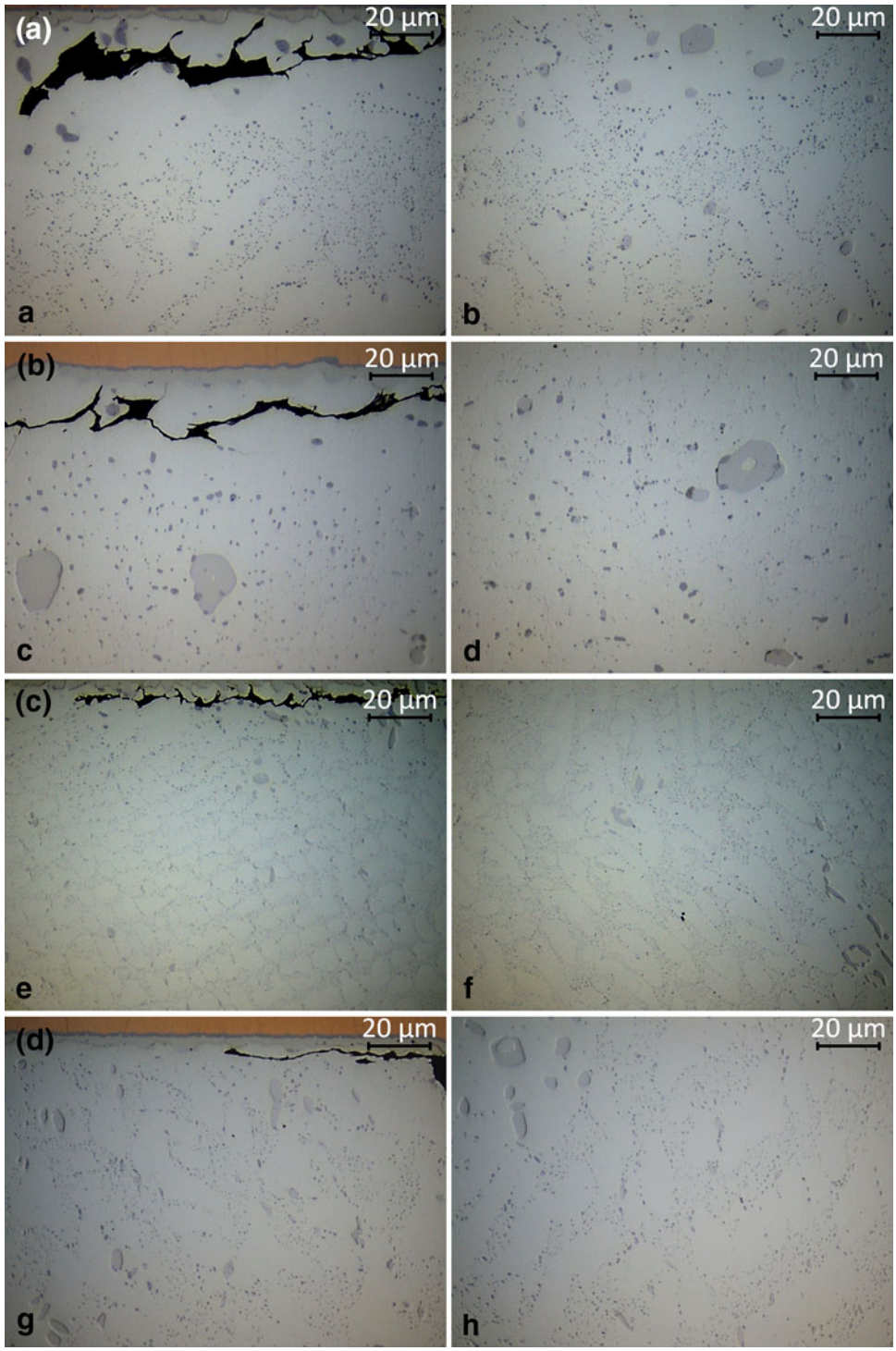

Fig. 4. Optical micrographs showing the microstructural evolution associated with crack propagation and evolution in the solder bulk: (a) highly accelerated conditions, (b) moderately accelerated conditions, (c) mildly accelerated conditions, and (d) nonaccelerated conditions. Letters in the lower left-hand corner indicate the magnification areas presented in Fig. 6.

surrounded by the network of high-angle grain boundaries. Low-angle grain boundaries can also be observed in the edge regions of the recrystallized volume. It is also noteworthy that the coarsening of the intermetallic particles is strong in the regions near the high-angle grain boundaries, while the regions near the low-angle boundaries still include finer particles, comparable to the bulk of the solder. This can be expected, as diffusion along high-angle boundaries is much faster than along low-angle boundaries. Similar findings have been reported in the literature by other groups.[16–19]

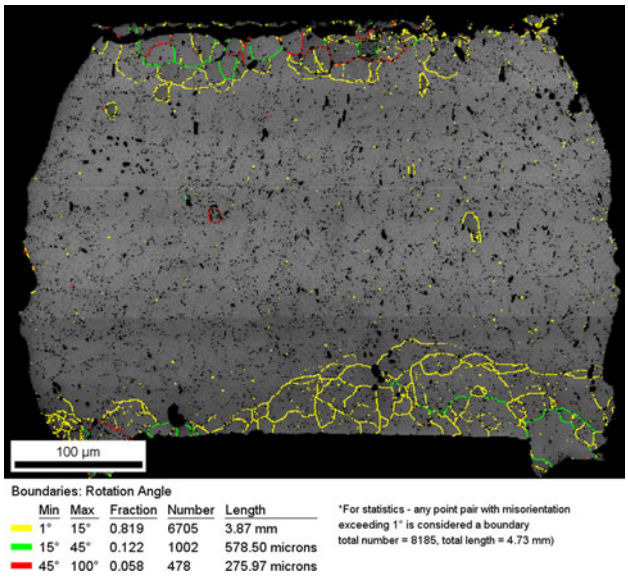

Fig. 5. EBSD map of a solder interconnection, showing grain boundaries with misorientation $<15°$ by yellow lines, 15° to 45° by green lines, and $>45°$ by red lines.

However, in the mildly/nonaccelerated conditions (green lifetime group), the microstructures have coarsened moderately in the vicinity of the crack region, but elsewhere the bulk microstructures are highly similar to the as-solidified microstructures (Fig. 4c, d). It is particularly noteworthy that recrystallization has not initiated under these conditions. Thus, the microstructural changes in the mildly/nonaccelerated conditions take place in a similar manner to under the highly accelerated conditions, but the microstructural evolution has not advanced to the stage where recrystallization is initiated. Under the moderately accelerated conditions (yellow lifetime group), the microstructural evolution had advanced further than under the mildly/nonaccelerated conditions, as early signs of recrystallization were occasionally observed. The microstructural evolution of the yellow lifetime group had characteristics of the evolution taking place in both the red and green lifetime groups without being clearly associated with either of them.

Crack Propagation and Fractographic Studies

The nucleation and propagation of cracks were investigated from the cross-sections and fracture surfaces of interconnections that were removed from the test chambers in the course of thermal cycling. The nucleation of cracks in the solder interconnections took place within a relatively narrow range, between about 500 and 1500 cycles, regardless of the test parameters used (see Refs. 20,21 for more details).

Failure analyses showed that, under the highly accelerated conditions (red lifetime group), the formation of the networks of grain boundaries by recrystallization had influenced the propagation of cracks (Fig. 6a). After the initiation of recrystallization, the recrystallized volume gradually expanded from the initial strain concentration regions over the interconnections, and cracks followed the expansion of the microstructurally changed volumes (as cracks grow, the distribution of stresses/strains evolves and the recrystallized volume expands). In such cases the cracks had not propagated further than the recrystallized region. Figure 7 shows fractographs of the failed solder interconnections. The highly accelerated failures exhibit a globular appearance of the surfaces as a result of the intergranular crack propagation between the recrystallized grains (Fig. 7a). Fatigue striations were occasionally observed on the surfaces of the recrystallized grains.[21] The networks of the grain boundaries formed by recrystallization evidently provide favorable paths for cracks to propagate intergranularly.

In the moderately accelerated conditions (yellow lifetime group) there was clearly less recrystallization than in the highly accelerated conditions, as shown in Fig. 6b (mostly rotation of the subgrains by recovery[22]). It was observed that cracks had propagated between the rotated region and the bulk solder. The appearances of the fracture surfaces were similar to those of the red lifetime group (Fig. 7b).

In the mildly/nonaccelerated conditions (green lifetime group), there was no recrystallization observed in the corner regions or in the crack area (Fig. 6c, d). Only slight subgrain rotation was observed in the edge regions of the solder interconnections (Fig. 6c). The mildly/nonaccelerated conditions showed cracking close to the IMC layer. The cracks had propagated transgranularly at the interface between the IMC layer and the bulk solder. The fracture surfaces of the mildly/nonaccelerated conditions (Fig. 7c, d) showed no globular appearance because the cracks had propagated transgranularly in the bulk solder.

Both in the moderately accelerated conditions and in the mildly/nonaccelerated conditions, the crack propagation rate was much slower as compared with the highly accelerated conditions where recrystallization-assisted crack propagation took place. It has been suggested earlier that the networks of grain boundaries formed by recrystallization provide favorable paths for cracks to propagate intergranularly with less energy consumption as compared with transgranular propagation (see Ref. 6 for more details). Comparison of the lifetime statistics and microstructural evolution of the different lifetime groups supports the suggestion that recrystallization significantly enhances the propagation rate of cracks under the thermal cycling conditions.

Based on the discussion above it seems that, in real-use environments, where the maximum temperatures rarely rise above 65°C,[23] the failure mechanism of recrystallization-assisted cracking is not initiated. Therefore, standardized tests that are used to assess the reliability of lead-free board

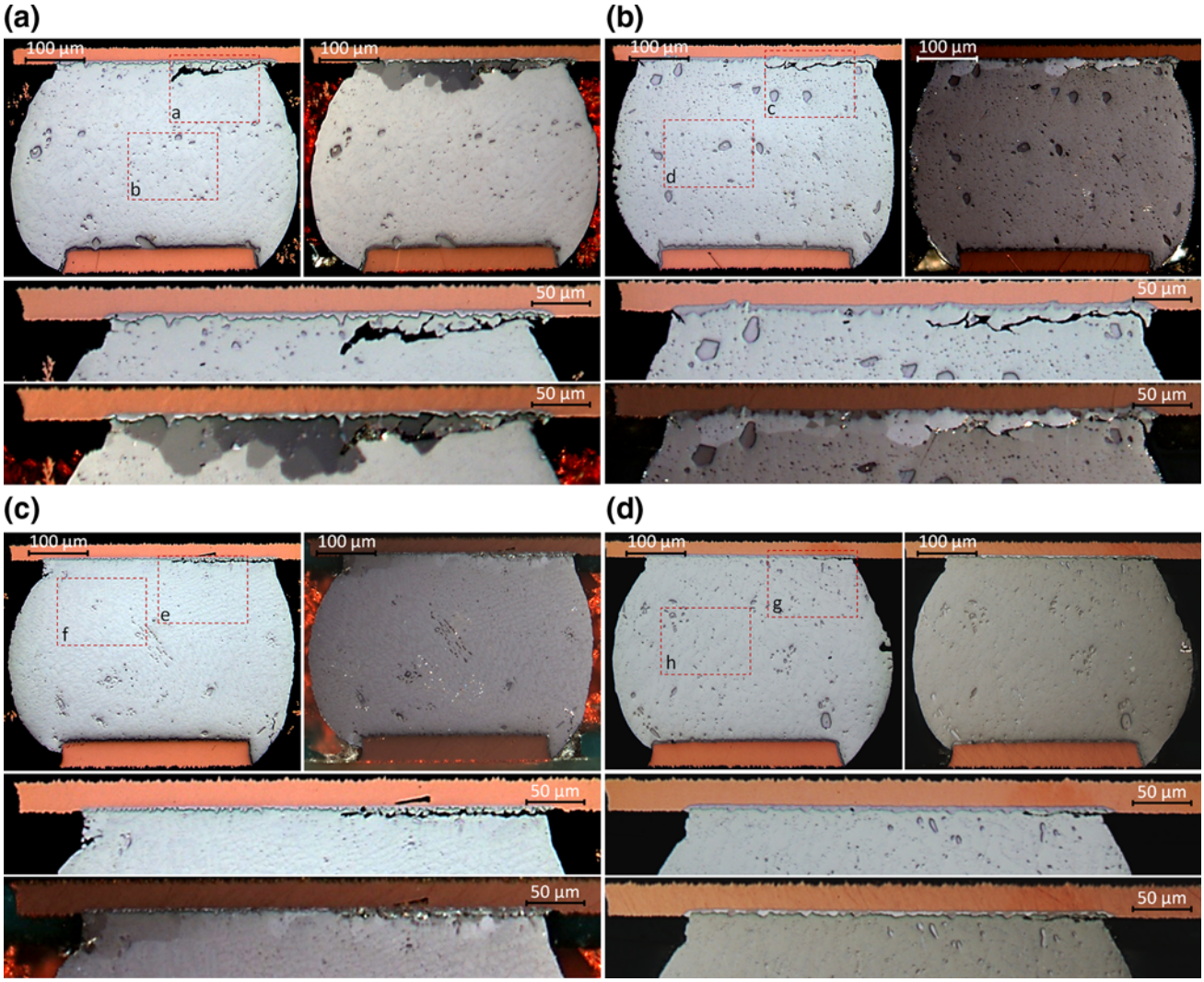

Fig. 6. A bright light image and a polarized light image showing the crack propagation in (a) highly accelerated conditions, (b) moderately accelerated conditions, (c) mildly accelerated conditions, and (d) nonaccelerated conditions. Dashed boxes indicate the locations of the magnified areas presented in Fig. 4.

assemblies produce a failure mechanism that is different from that produced in real-use environments.

DISCUSSION

The results of this work show that the failures of solder interconnections are dependent on the evolution of their microstructures (see Table II for summary). In this section, we attempt to formalize our understanding of the observed failure mechanisms and to answer why the failure mechanism is different under the accelerated and real-use conditions. In addition to the growth and coarsening of IMC particles and the primary tin cells, there are microstructural changes (produced by recovery and recrystallization) that are driven by the plastic deformation of solder interconnections. The significance of the microstructural changes depends on how much driving force is produced under different thermal cycling loading conditions. The driving force of recovery and recrystallization is the energy stored (in the form of defects) in the crystal structures during plastic deformation, but the activation energy of recovery is much lower as compared with that of recrystallization. The onset of recrystallization and what kind of microstructural changes take place depend on how much of this stored energy is released by recovery and how much by recrystallization. Recovery is the rearrangement of dislocations and, therefore, occurs relatively quickly, while recrystallization starts after an incubation period. Thus, recrystallization is initiated only if the cyclic accumulation of stored energy is faster than its release by recovery. The observed differences in the microstructural evolution can therefore be explained by the (im)balance of accumulation of stored energy

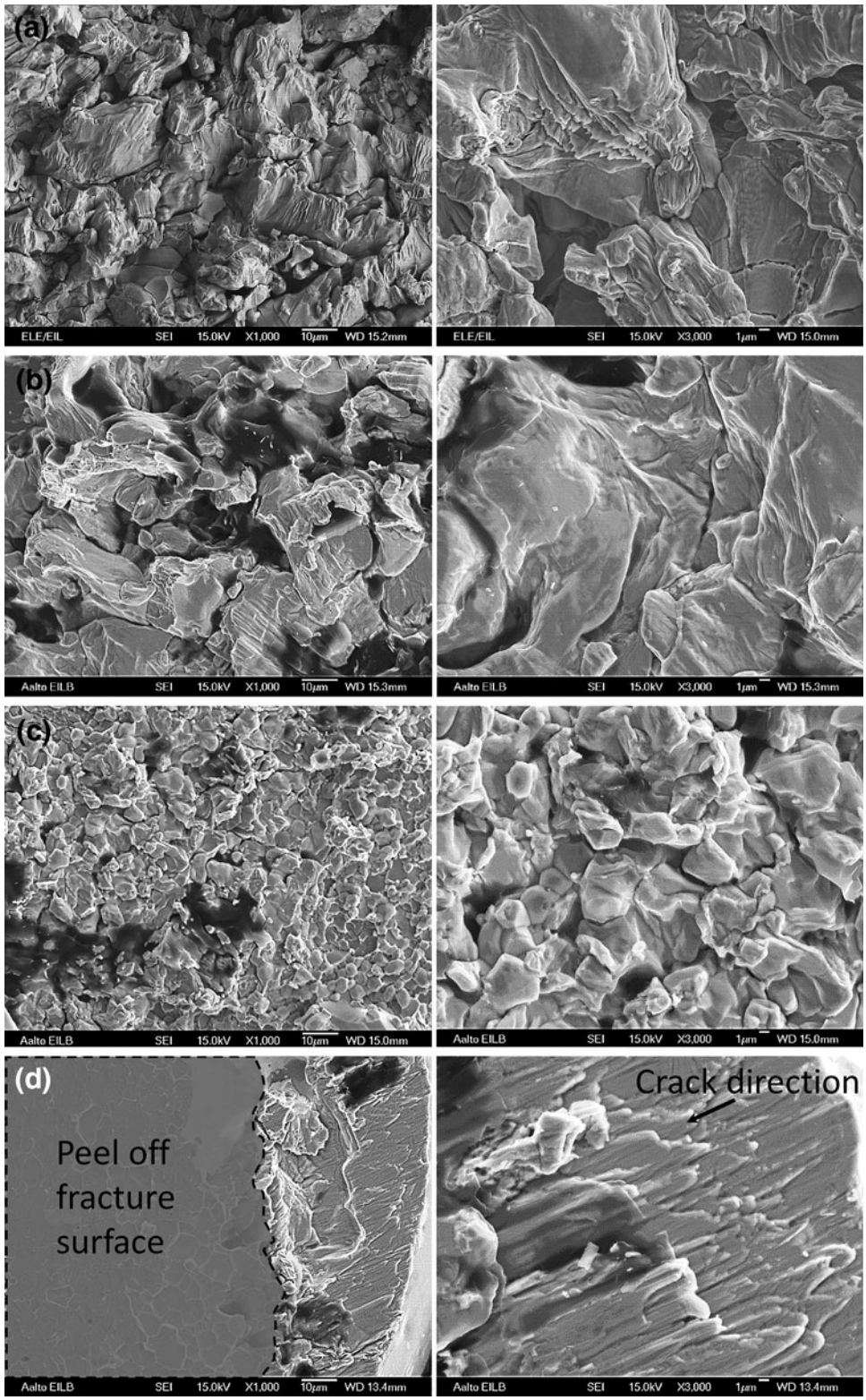

Fig. 7. Fractographs of the solder interconnections viewed from the component side: (a) highly accelerated conditions, (b) moderately accelerated conditions, (c) mildly accelerated conditions, and (d) nonaccelerated conditions (the fracture surface caused by the peel-off is blurred in grey color).

produced by cyclic deformation and the release of this energy by recovery and recrystallization under the different thermal cycling conditions. The results indicate that, under real-use conditions, the accumulation of stored energy is relatively low (modest plastic deformation of solder) and recovery appears to

Table II. Summary of the observed failure mechanisms associated with the three lifetime groups

Lifetime group (acceleration class)	Bulk microstructure: 1) region of strain concentration 2) centre of the interconnection	Macrostructure (recrystallization)	Crack propagation	Test duration (time-to-failure)
Highly accelerated conditions	1) Major coarsening of the IMC particles (cellular structure disappeared completely) 2) Coarsening of the IMC particles	Recrystallization over the entire interconnection area	Intergranular bulk solder cracking (recrystallization assisted)	< 10 000 h
Moderately accelerated conditions	1) Coarsening of the IMC particles (cellular structure disappeared) 2) Coarsening of the IMC particles	Rotation of sub-grains (early stage of recrystallization) in the edge regions and in the proximity of the cracks	Cracking between the as-solidified and changed micro-structures	> 20 000 h
Mildly / Non-accelerated conditions	1) Slight coarsening of the IMC particles (in the vicinity of the crack) 2) Similar to the as-solidified microstructure	Rotation of sub-grains in the edge regions	Transgranular cracking at the interface between the IMC and the bulk solder Transgranular bulk solder cracking	>> 25 000 h

release the majority of this energy while recrystallization is not initiated. On the other hand, under the highly accelerated conditions (significant plastic deformation), the driving force is accumulated faster than it is released by recovery, and therefore, recrystallization is initiated to assist the release of stored energy. However, the initiation of recrystallization has significant consequences for the lifetime of solder interconnections, since the recrystallized microstructures appear to crack easily. Therefore, we have a reason to believe that the failure mechanism caused by the highly accelerated conditions does not reproduce the same failure mechanism that is produced under real-use conditions.

As these results show, increasing the difference between the extreme temperatures is an effective way to accelerate thermal cycling, but attention should be paid to the mean temperature of the thermal cycle. The results show that the upper temperature should not be increased beyond about 75°C to 100°C, and therefore the only possibility to increase ΔT is to reduce the lower extreme temperature. The results show that, contrary to popular opinion, the accumulation of microstructural damage during the lower-temperature section of a thermal cycle is significant and the low temperature contributes significantly to the acceleration of failures. However, as shown by the lifetime statistics, this leads to significantly longer test duration (compared with tests carried out with higher mean temperatures). However, one can also argue that, in this way, the failure mechanisms produced and resulting lifetimes are representative of products in real-use conditions.

CONCLUSIONS

Lifetimes and fracture mechanisms of solder interconnections under cyclic conditions were found to be dependent on the parameters of the thermal cycling tests. Test conditions representing normal changes of temperature (e.g., inside modern portable electronic products) induced much longer lifetimes as well as fracture mechanisms that differed greatly from those observed under the highly accelerated test conditions. In the accelerated tests, the microstructural evolution (recrystallization) controlled the propagation of cracks, while in the real-use conditions, significantly less microstructural evolution took place and the rate of crack propagation through the solder was notably lower. Under the standardized thermal cycling conditions (highly accelerated conditions), the networks of grain boundaries formed by recrystallization provided favorable paths for cracks to propagate intergranularly. It is noteworthy that the coarsening of intermetallic particles was strong in the recrystallized regions (the cellular structure had disappeared completely in the crack region). However, under the real-use conditions (mildly/nonaccelerated conditions), recrystallization was not observed in the solder interconnections and cracks had propagated transgranularly in the bulk solder. The real-use conditions showed slight coarsening of the microstructure close to the crack, but the solder bulk still included finer IMC particles. These findings suggest that standardized thermal cycling tests that are used to assess the solder interconnection reliability of BGA144 component boards create failure mechanisms that are not seen in conditions

representing real-use operation. Therefore, alternative test parameters should be used instead of those defined in the standard thermal cycling tests. One solution to produce the same failure mechanism as the real-use conditions is to lower the mean temperature of the thermal cycling tests. Microstructural changes that correlate with real-use conditions should also be incorporated into lifetime prediction models and lifetime estimations.

ACKNOWLEDGEMENTS

The authors would like to thank the Academy of Finland and Nokia Siemens Networks for their financial support. Mr. Otso Ratia is acknowledged for his help with the experimental work.

REFERENCES

1. S. Nurmi, J. Sundelin, E. Ristolainen, and T. Lepistö, *Microelectron. Reliab.* 44, 485 (2004).
2. J.W. Morris Jr, D. Tribula, T.S.E. Summers, and D. Grivas, *Solder Joint Reliability*, ed. J.H. Lau (New York: Van Nostrand Reinold, 1991), pp. 225–265.
3. J.W. Morris Jr, D. Grivas, D. Tribula, T. Summers, and D. Frear, *Solder. Surf. Mt. Technol.* 1, 4 (1989).
4. T.T. Mattila, T. Laurila, and J.K. Kivilahti, *Micro-and Opto-Electronic Materials and Structures: Physics, Mechanics, Design, Reliability and Packaging*, ed. E. Suhir, C.P. Wong, and Y.C. Lee (New York: Springer, 2007), pp. 313–350.
5. T.T. Mattila and J.K. Kivilahti, *IEEE Trans. Compon. Packag. Technol.* 33, 629 (2010).
6. T.T. Mattila and J.K. Kivilahti, *Recrystallization*, ed. K. Sztwiertnia (Intech Open Access, 2012). doi:10.5772/37899.
7. L. Lehman, S. Athavale, T. Fullem, A. Giamis, R. Kinyanjui, M. Lowenstein, K. Mather, R. Patel, D. Rae, J. Wang, Y. Xing, L. Zavalij, P. Borgesen, and E. Cotts, *J. Electron. Mater.* 33, 1429 (2004).
8. T.T. Mattila, V. Vuorinen, and J.K. Kivilahti, *J. Mater. Res.* 19, 3214 (2004).
9. D. Henderson, J.J. Woods, T.A. Gosseling, J. Bartelo, D.E. King, T.M. Korhonen, M.A. Korhonen, L.P. Lehman, E.J. Cotts, S.K. Kang, P. Lauro, D.-Y. Shih, C. Goldsmith, and K.J. Puttliz, *J. Mater. Res.* 19, 1608 (2004).
10. S. Terashima, K. Takahama, M. Nozaki, and M. Tanaka, *Mater. Trans.* 45, 1383 (2004).
11. S. Dunford, S. Canumalla, and P. Viswanadham, *Proc. 54th Electron. Compon. Technol. Conf.* (Piscataway, NJ: IEEE, 2004), pp. 726–736.
12. J.J. Sundelin, S.T. Nurmi, and T.K. Lepistö, *Mater. Sci. Eng. A* 474, 201 (2008).
13. H. Chen, M. Mueller, T.T. Mattila, J. Li, X. Liu, K.J. Wolter, and M. Paulasto-Kröckel, *J. Mater. Res.* 26, 2103 (2011).
14. L. Yin, L. Wentlent, L. Yang, B. Arfaei, A. Oasaimeh, and P. Borgesen, *J. Electron. Mater.* 41, 241 (2012).
15. T.T. Mattila, M. Mueller, M. Paulasto-Kröckel, and K.J. Wolter, *Proc.* 3rd *Electro. Syst. Integr. Technol. Conf.* (Piscataway, NJ: IEEE, 2010), pp. 1–8.
16. S. Terashima, T. Kohno, A. Mizusawa, K. Arai, O. Okada, T. Wakabayashi, M. Tanaka, and K. Tatsumi, *J. Electron. Mater.* 38, 33 (2009).
17. H. Chen, J. Han, and M. Li, *J. Electron. Mater.* 40, 2470 (2011).
18. T.R. Bieler, B. Zhou, L. Blair, A. Zamiri, P. Darbandi, F. Pourboghrat, T.-K. Lee, and K.-C. Liu, *J. Electron. Mater.* 41, 283 (2012).
19. B. Zhou, T.R. Bieler, T.-K. Lee, and W. Liu, *J. Electron. Mater.* (2012). doi:10.1007/s11664-012-2307-z.
20. T. T. Mattila, H. Xu, O. Ratia, and M. Paulasto-Kröckel, *Proc. 60th Electron. Compon. Technol. Conf.* (Piscataway, NJ: IEEE, 2010), pp. 581–590.
21. H. Xu, O. Ratia, J. Hokka, T.T. Mattila, and M. Paulasto-Kröckel, *IEEE Trans. Comp. Packag. Manuf. Technol.* (in print).
22. A.U. Telang, T.R. Bieler, A. Zamiri, and F. Pourboghrat, *Acta Mater.* 55, 2265 (2007).
23. J.S. Karppinen, J. Li, T.T. Mattila, and M. Paulasto-Kröckel, *Microelectron. Reliab.* 50, 1994 (2010).